Identification and Multivariable Iterative Learning Control of an RTP Process for Maximum Uniformity of Wafer Temperature

Moonki Cho[1], Yonghee Lee[2] , Sangrae Joo[3], and Kwang S. Lee[2]

[1] Conwell Co. Ltd, Seoul, Korea
(Tel : +82-2-529-4802; E-mail: iloveyou@conwell.co.kr)
[2] Dept. Chem. Engng., Sogang Univ., Seoul, Korea
(Tel : +82-2-705-8477; E-mail: abraxase@sogang.ac.kr , kslee@ccs.sogang.ac.kr)
[3] Kornic Systems Co. , Suwon, Korea
(Tel : +82-31-379-2750; E-mail: srjoo@kornic.co.kr)

Abstract: Comprehensive study on the control system design for a RTP process has been conducted. The purpose of the control system is to maintain maximum temperature uniformity across the silicon wafer achieving precise tracking for various reference trajectories. The study has been carried out in two stages: thermal balance modeling on the basis of a semi-empirical radiation model, and optimal iterative learning controller design on the basis of a linear state space model. First, we found through steady state radiation modeling that the fourth power of wafer temperatures, lamp powers, and the fourth power of chamber wall temperature are related by an emissivity-independent linear equation. Next, for control of the MIMO system, a state space model- and LQG-based two-stage batch control technique was derived and employed to reduce the heavy computational demand in the original two-stage batch control technique. By accommodating the first result, a linear state space model for the controller design was identified between the lamp powers and the fourth power of wafer temperatures as inputs and outputs, respectively. The control system was applied to an experimental RTP equipment. As a consequence, great uniformity improvement could be attained over the entire time horizon compared to the original multi-loop PID control. In addition, controller implementation was standardized and facilitated by completely eliminating the tedious and lengthy control tuning trial.

Keywords: Rapid Thermal Process, Iterative Learning Control, Run-to-Run Control, LQG Control

1. INTRODUCTION

In the study of RTP systems, the most important issue is how to achieve a uniform temperature profile across the wafer surface while tracking a specified temperature trajectory as closely as possible. To overcome this problem, much research effort has been made in both the design and control aspects [1,2,3]. For the design side, a few to several patented design concepts are dominating the commercial market. For the control side, however, there seem to remain still many issues to improve from temperature sensing to control techniques. As the standard size of the silicon wafer has grown from 6 inches to 8 inches and is now moving to 12 inches, and also the feature size of the IC pattern decreases continuously, issues from control continuously pose new challenges.

From the system theoretic point of view, the RTP system can be considered a nonlinear, multivariable batch system with fast dynamics and noisy measurements where highly accurate tracking over a range of several hundred degrees of Celsius or more is required. Moreover, a single RTP system can be used for different wafer processings under different temperatures profiles and the characteristics of an RTP system slowly vary by contamination. Reliable modelling of the system under such an operational environment is quite demanding. For such systems, therefore, traditional model-based MIMO

(Multi-Input Multi-Output) control techniques may show limited performance because of their strong model dependency. Such a problem is manifest from the previous studies [4,5,6,7,8,9,10].

To overcome the above mentioned problem, Lee et al. [11] have devised the so-called BLQG (Batch LQG) technique. BLQG is an LQG version of the BMPC technique for faster computation in an unconstrained batch process control problem. As the run number increases, both methods attain asymptotically minimum achievable tracking error getting over model uncertainty unless there is random disturbance. The key feature to make this possible is the embedded batch-wise integral feedback control action in the control techniques. Along with the control algorithm, Lee et al. [11] have suggested an easy and efficient time-varying linear model construction technique for RTP systems that may approximate the inherent nonlinear behavior. The proposed technique has been applied to an experimental RTP system for 8 inch wafers and showed excellent performance [12].

In this paper, with a purpose to further enhance the previous studies, we have first investigated the thermal balance relationship and proposed a control-relevant model structure of the RTP system. The model is represented by a linear dynamic relation combined with a nonlinear static output map. Next, a new two-stage batch control (TBC) technique based on a state space model and LQG control was derived to reduce the heavy computational demand in the original two-stage batch control technique [14]. The RTP control system was designed on the basis of the new state space model and the new TBC technique. The control system was applied to a prototype RTP equipment.

2. DESCRIPTION OF THE EXPERIMENTAL RTP SYSTEM

The RTP system concerned in this study is shown in Fig. 1. The silicon wafer is heated by an array of 38 tungsten-halogen lamps whose maximum power is 1 Kw each. The lamps are assembled together by two or three to make total ten independent groups. The chamber wall has a cooling water circulation path inside. For parameter estimation of the thermal balance model, temperatures are measured at eight locations on the wafer surface. As a consequence, the RTP system is configured as a 8x10 MIMO system. The National Instrument boards are used for data interface and the application software was developed with LabView for

SCADA and Matlab script. To compensate for the power fluctuation, an AVR-like system was devised using PI controllers. The overall batch horizon for each experiment was chosen to 45 sec with the sampling time of 0.5 sec. The reference temperature trajectory consists of a holding zone at 400℃ for 7 sec and a ramping zone with 50℃/sec followed by a holding zone at 800℃ for 25 sec.

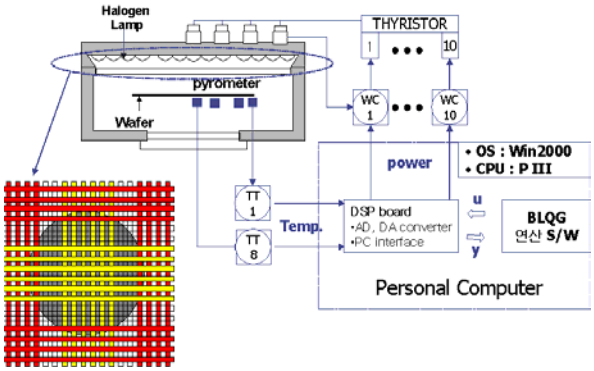

Fig. 1. Schematic diagram of the RTP system and computer interface.

3. THERMAL BALANCE MODELING

3.1 Basic Radiation Equations

We shall assume that all surfaces considered in our analysis are *gray, diffuse* and *opaque*. Also the emissive and reflective properties of each surface are not spatially distributed although it may be temperature-dependent.

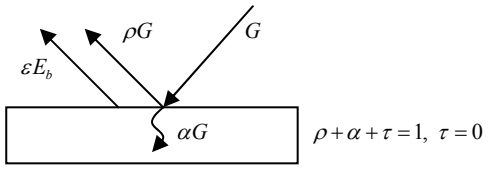

J : Radiosity G : Irradiation

Fig. 2. Sketch showing effects of incident radiation/

As depicted in Fig. 2, if G represents the *irradiation* (incident radiation energy per unit area), the radiosity J (total radiant emission per unit area) for an opaque surface is represented by

$$J = \varepsilon E_b + (1-\varepsilon)G \tag{1}$$

In the above $E_b = \sigma T^4$ represents the black-body emissive power where σ is the Stefan-Boltzman constant. The net radiation heat flow from the surface of area A is, therefore,

$$q = A(J-G) = \frac{\varepsilon A}{1-\varepsilon}(E_b - J) \tag{2}$$

Now consider the exchange of radiant energy between two surfaces A_1 and A_2. Of that total radiation which leaves surface 1, the amount that reaches surface 2 is $F_{21}A_1J_1$ and the reverse is $F_{12}A_2J_2$ where F_{ij} is the view factor from surface j to surface i. By the reciprocity relationship, it holds that $F_{ji}A_i = F_{ij}A_j$ for any i and j. The net interchange between the two surfaces is, therefore,

$$q_{21} = F_{21}A_1(J_1 - J_2) = F_{12}A_2(J_1 - J_2) \tag{3}$$

Note that the index for the view factor is reversed from the usual convention. It is for convenience in the vector notations that will be introduced later.

3.2 Steady State Thermal Balance Model for the RTP Process

For thermal balance modeling of the RTP process, we first divide the wafer and chamber wall into small segments over each of which the temperature can be considered to be constant. The lamp array surface is divided according to the ten pre-assembled groups. Let the indices s, w, and l be used to indicate the segment of the silicon wafer, chamber wall, and lamp surfaces, respectively. First, the net radiant heat input on the wafer segment s is represented as

$$q_s = \sum_l \left(F_{sl}A_lJ_l - F_{ls}A_sJ_s\right) + \sum_w \left(F_{sw}A_wJ_w - F_{ws}A_sJ_s\right) + \sum_{s'} \left(F_{ss'}A_sJ_{s'} - F_{s's}A_sJ_s\right) \tag{4}$$

where s' denotes a wafer segment other than s. From (2), the net radiant heat input can also be written as

$$q_s = = \frac{\varepsilon(T_s)A_s}{1-\varepsilon(T_s)}\left(J_s - E_{bs}(T_s)\right) \tag{5}$$

To simplify the representation, let us introduce the following vector and matrix notations:

$$\mathbf{q}_s = \begin{bmatrix} q_1 \\ \vdots \\ q_{n_s} \end{bmatrix}, \mathbf{V}_{sl} = \begin{bmatrix} F_{11}A_1 \cdots F_{1n_l}A_{n_l} \\ \vdots \ \ddots \ \vdots \\ F_{1n_s}A_1 \cdots F_{n_sn_l}A_{n_l} \end{bmatrix}, \mathbf{A}_s = \begin{bmatrix} \frac{\varepsilon_1 A_1}{(1-\varepsilon_1)} & \cdots & 0 \\ \vdots & \ddots & \vdots \\ 0 & \cdots & \frac{\varepsilon_{n_s}A_{n_s}}{(1-\varepsilon_{n_s})} \end{bmatrix},$$

$$\Pi_{ss} \triangleq \begin{bmatrix} \left(\sum_l F_{l1} + \sum_c F_{c1} + \sum_{s'} F_{s'1}\right)A_1 \cdots & 0 \\ \vdots & \ddots \ \vdots \\ 0 & \cdots \left(\sum_l F_{ln_s} + \sum_c F_{cn_s} + \sum_{s'} F_{s'ln_s}\right)A_{n_s} \end{bmatrix} \tag{6}$$

Other vectors $\mathbf{J}$'s and $\mathbf{E}_b$'s are defined similarly to $\mathbf{q}_s$. Also other matrices $\mathbf{V}$'s, $\mathbf{A}$'s, and Π's are defined similarly to $\mathbf{V}_{sl}$, $\mathbf{A}_s$, and Π_{ss}, respectively. In (6), the indices of the elements in the vector and matrices follow the indices of the vector and matrices, *i.e.*, $q_1 = q_{s=1}$, $F_{11}A_1 = F_{s=1,l=1}A_{l=1}$ and so forth. Using the vector notation, (4) and (5) can be rewritten as

$$\mathbf{q}_s = \mathbf{A}_s(\mathbf{J}_s - \mathbf{E}_{bs}) = \mathbf{V}_{sl}\mathbf{J}_l + \mathbf{V}_{sw}\mathbf{J}_w + (\mathbf{V}_{ss} - \Pi_{ss})\mathbf{J}_s \tag{7}$$

In the similar manner, the radiant heat flow for the chamber wall and the lamps can be written as

$$\mathbf{q}_w = \mathbf{A}_w(\mathbf{J}_w - \mathbf{E}_{bw}) = \mathbf{V}_{cl}\mathbf{J}_l + \mathbf{V}_{ws}\mathbf{J}_s + (\mathbf{V}_{cc} - \Pi_{cc})\mathbf{J}_w \tag{8}$$

$$\mathbf{q}_l = \mathbf{A}_l(\mathbf{J}_l - \mathbf{E}_{bl}) = \mathbf{V}_{lc}\mathbf{J}_c + \mathbf{V}_{ls}\mathbf{J}_s + (\mathbf{V}_{ll} - \Sigma_{ll})\mathbf{J}_l \tag{9}$$

In the above, the heat flow from each lamp group is equivalent to the electric power applied to the lamp group. If we represent the applied powers to the lamp groups as $\mathbf{p}$,

$$\mathbf{p} = \mathbf{q}_l \tag{10}$$

Under a steady state, the net heat flow from each wafer segment is zero. Hence,

$$\mathbf{q}_s = \mathbf{0} \Leftrightarrow \mathbf{J}_s = \mathbf{E}_{bs} = \sigma\mathbf{T}_s^4 \tag{11}$$

where $\mathbf{T}_s^4 = [T_1^4 \ \cdots \ T_{n_s}^4]^T$. Also the heat carried by the cooling water per unit time is equal to the negative sum of the elements of $\mathbf{q}_w$. Substitution of (10) and (11) into (7) to (9) and rearrangement gives the following:

$$\mathbf{0} = \mathbf{V}_{sl}\mathbf{J}_l + \mathbf{V}_{sw}\mathbf{J}_w + (\mathbf{V}_{ss} - \Pi_{ss})\mathbf{E}_{bs} \tag{12}$$

$$\mathbf{A}_w(\mathbf{J}_w - \mathbf{E}_{bw}) = \mathbf{V}_{cl}\mathbf{J}_l + (\mathbf{V}_{cc} - \Pi_{cc})\mathbf{J}_w + \mathbf{V}_{ws}\mathbf{E}_{bs} \quad (13)$$

$$\mathbf{p} = (\mathbf{V}_{ll} - \mathbf{\Sigma}_{ll})\mathbf{J}_l + \mathbf{V}_{lc}\mathbf{J}_c + \mathbf{V}_{ls}\mathbf{E}_s \quad (14)$$

Since the chamber wall temperature T_w is measurable, $\mathbf{E}_{bw}$ is known. Hence, there remain three unknown variables $\mathbf{J}_w$, $\mathbf{J}_l$, and $\mathbf{E}_{bs}$ and we have three linear equations. This implies that $\mathbf{E}_{bs}$ can be represented as a linear combination of $\mathbf{p}$ and $\mathbf{E}_{bw}$ such as

$$\mathbf{E}_{bs} = \mathbf{D}\mathbf{p} + \mathbf{B}\mathbf{E}_{bw} \Leftrightarrow \mathbf{T}_s^4 = \mathbf{D}\mathbf{p} + \mathbf{B}\mathbf{T}_w^4 \quad (15)$$

If $\mathbf{p} = 0$, T_s under the thermal equilibrium should be equal to T_w. This restricts $\mathbf{B}$. Moreover if the chamber wall temperature is not distributed but uniform over the whole surface, then (15) can be simplified to

$$\mathbf{T}_s^4 = \mathbf{D}\mathbf{p} + \mathbf{E}\mathbf{T}_w^4 \quad (16)$$

where $\mathbf{E} = [1 \ \cdots \ 1]^T$. From (12) to (14), $\mathbf{D}$ is a matrix independent of the emissivity of the silicon wafer and tungsten-halogen lamp. The shape factors are invariant. Thus if the chamber wall emissivity is constant, which is reasonable since T_w doesn't change much, $\mathbf{D}$ becomes a constant matrix. Indeed, $\mathbf{D}$ can be further restricted by the facts that $\mathbf{V}_{ls} = \mathbf{V}_{sl}^T$ and likewise for other $\mathbf{V}$'s, and the three equations (7) to (9) become zero when $\mathbf{p} = 0$. However, the structural restrictions by these relations are too complicated to accommodate. We may neglect them and determine $\mathbf{D}$ through experiments. Originally, $\mathbf{T}_s^4$ in (16) contains the temperatures of the wafer segments that cover the entire wafer surface. However, (16) also holds for $\mathbf{T}_s^4$ that is composed of only the measured temperatures if $\mathbf{D}$ is considered as the partition of the original $\mathbf{D}$ that corresponds to the measured temperatures.

4. CONTROL MODEL

In the previous section, it has been shown that the steady state thermal balance of an RTP system is represented by a linear (more accurately affine) relationship between the lamp powers and the fourth power of the wafer temperatures as in (15). Extending this relationship to the dynamic case where lamp groups $p(t) \in \mathbb{R}^{n_u}$ and a part of $\mathbf{T}_s^4$, say $T_{s,con}^4 \in \mathbb{R}^{n_y}$, are used as the manipulated variable and the controlled variable, respectively, we have

$$\begin{aligned} x(t+1) &= Ax(t) + Bu(t) + Kv(t) \\ y(t) &= Cx(t) + v(t) \end{aligned} \quad (17)$$

where $u(t) = p(t)$ and $y(t) \triangleq T_{s,con}^4(t)$. (A, B, C) can be found using a subspace identification technique like N4SID. To remove the bias effect (e.g., by T_w^4) and while appropriately suppressing the high frequency amplification, it is recommended to filter $u(t)$ and $y(t)$ using $F(q^{-1}) = (1-q^{-1})/(1-fq^{-1}), 0 < f < 1$ before processing by the identification technique. In (17), $v(t)$ represents the bias term together with other disturbance effects. Hence (17) is not in a rigorous sense a standard linear stochastic state space equation where $v(t)$ is a zero-mean white noise sequence. It is true that (17) may not properly represent the RTP dynamics. But the steady state behavior can be quite reasonably represented by (17) over a wide temperature range with constant system matrices.

5. TWO-STAGE OPTIMAL BATCH CONTROL TECHNIQUE

The two-stage batch control (TBC) technique is a very recent iterative learning control (ILC) technique combined with real-time feedback control (RFC)[14]. It has been developed to solve the following chronic problem of the traditional ILC-RFC techniques: The present ILC-RFC techniques can be described by the following general formulation:

$$u_k(t) = u_{k-1}(t) + \mathrm{H}_1 e_{k-1}(1:N) + \mathrm{H}_2 e_k(1:t) \quad (18)$$

where the subscript k denotes the run index; e_k is the control error; $(i:j)$ means data from $t = i$ to j; k represents the run index; H_1 and H_2 represent the gains for ILC and RFC, respectively. As can be imagined, when there enters a large real-time disturbance, it necessarily move $u_k(t)$ away from $u_{k-1}(t)$ and control performance over the next few to several batches suffer from the bad batch. The TBC technique separates $u(t)$ into the ILC and RFC parts so that the real-time disturbance doesn't have effects on the ILC input. The present TBC technique is based on an FIR model description and predictive control .

The TBC technique proposed in this research is a modification of the existing one in that it is based on a state space model and the LQG (Linear Quadratic Gaussian) method is used for RFC. The major motivation for this is to reduce the computation required in real-time. In addition, frequency domain tuning and blocking techniques are introduced to the ILC part to diminish the required computation after each batch run.

5.1 Model Recasting for TBC Formulation

In (17), due to the bias term, model error effects, and others, $v_k(t)$ may exhibit persistent or drifting behavior along k in addition to random fluctuations. Such behavior can be reasonably modeled by the equation

$$v_k(t) = \overline{v}_k(t) + \hat{v}_k(t), \ \overline{v}_k - \overline{v}_{k-1}(t) = n_k(t) \quad (19)$$

We assume that $\hat{v}_k(t)$ and $n_k(t)$ are independent random sequences with respect to both k and t indices.

Now, we decompose $u_k(t)$ into $\overline{u}_k(t)$ and $\hat{u}_k(t)$, and decompose (17) into two parts, one that is driven by $\overline{u}_k(t)$ and $\overline{v}_k(t)$, and the other driven by $\hat{u}_k(t)$ and $\hat{v}_k(t)$.

$$\begin{aligned} \overline{x}_k(t+1) &= A\overline{x}_k(t) + B\overline{u}_k(t) + K\overline{v}_k(t) \\ \overline{y}_k(t) &= C\overline{x}_k(t) + \overline{v}_k(t) \end{aligned} \quad (20)$$

$$\begin{aligned} \hat{x}_k(t+1) &= A\hat{x}_k(t) + B\hat{u}_k(t) + K\hat{v}_k(t) \\ \hat{y}_k(t) &= C\hat{x}_k(t) + \hat{v}_k(t) \end{aligned} \quad (21)$$

Of course, $y_k(t) = \overline{y}_k(t) + \hat{y}_k(t)$.

In order to put (20) into the standard form in which the external noise is an independent sequence in terms of k as well as t, we first take the difference on the equations for two consecutive runs to obtain

$$\begin{aligned} \Delta\overline{x}_k(t+1) &= A\Delta\overline{x}_k(t) + B\Delta\overline{u}_k(t) + Kn_k(t) \\ \overline{y}_k(t) &= C\Delta\overline{x}_k(t) + \overline{y}_{k-1}(t) + n_k(t) \end{aligned} \quad (22)$$

where $\Delta\overline{x}_k \triangleq \overline{x}_k - \overline{x}_{k-1}$ and $\Delta\overline{u}_k \triangleq \overline{u}_k - \overline{u}_{k-1}$

5.2 Computation Sequence of the TBC Algorithm

The TBC algorithm is run as follows;

• Assume that the $k-1^{th}$ batch operation is finished and $\{e_{k-1}(t), \overline{u}_{k-1}(t), \hat{u}_{k-1}(t)\}$ are available where

$e_k(t) \triangleq r(t) - y_k(t)$ and $r(t)$ is the reference trajectory for $y_k(t)$

• *ILC Computation*: Calculate $\bar{u}_k(t)$ such that a cost function for $\bar{e}_{k|k-1}(t)$ is minimized.

• Assume that the k^{th} batch operation is started

• *RFC Computation*: At t in the k^{th} batch operation, calculate the real-time control input $\hat{u}_k(t)$ such that $e_k(t)$ is properly regulated.

5.3 ILC Formulation

Since ILC computation is based on the output prediction, it is necessary to derive the predictor equation. For this we define

$$\bar{\mathbf{e}} \triangleq \left[\bar{e}(1)^T \quad \bar{e}(2)^T \quad \cdots \quad \bar{e}(N)^T\right]^T$$

$$\Delta\bar{\mathbf{u}} \triangleq \left[\Delta\bar{u}(0)^T \quad \Delta\bar{u}(1)^T \quad \cdots \quad \Delta\bar{u}(N-1)^T\right]^T$$

$$\mathbf{n} \triangleq \left[n(1)^T \quad n(1)^T \quad \cdots \quad n(N)^T\right]^T \tag{23}$$

where $\bar{e}(t) = r(t) - \bar{y}(t)$ and similarly for other variables. If we write the output error prediction for the $k+1^{th}$ batch as a function of $\Delta\bar{\mathbf{u}}_{k+1}(t)$ using (22) and collect them in a vector form, we have

$$\bar{\mathbf{e}}_{k+1} = \bar{\mathbf{e}}_k - \mathbf{G}\Delta\bar{\mathbf{u}}_{k+1} - \underbrace{(\mathbf{F}\mathbf{n}_{k+1} + \mathbf{M}\Delta\bar{x}_{k+1}(0))}_{\mathbf{w}_{k+1}} \tag{24}$$

where

$$\mathbf{G} \triangleq \begin{bmatrix} CB & 0 & \cdots & 0 \\ CAB & CB & \cdots & 0 \\ \vdots & \vdots & \ddots & \vdots \\ CA^{N-1}B & CA^{N-2}B & \cdots & CB \end{bmatrix} \tag{25}$$

Similarly from (21),

$$\hat{\mathbf{y}}_k = \mathbf{G}\hat{\mathbf{u}}_k + \mathbf{F}\hat{\mathbf{v}}_k + \mathbf{M}\hat{x}_k(0) \tag{26}$$

Since $e = r - y = \bar{e} - \hat{y}$, we have

$$\mathbf{e}_k = \bar{\mathbf{e}}_k - \mathbf{G}\hat{\mathbf{u}}_k - \mathbf{F}\hat{\mathbf{v}}_k - \mathbf{M}\hat{x}_k(0)$$

$$\Rightarrow \mathbf{e}_k + \mathbf{G}\hat{\mathbf{u}}_k = \hat{\mathbf{e}}_k - \underbrace{(\mathbf{F}\hat{\mathbf{v}}_k + \mathbf{M}\hat{x}_k(0))}_{\mathbf{m}_k} \tag{27}$$

Now, on the basis of (24) and (27), the Kalman filter equation is given as

$$\bar{\mathbf{e}}_{k|k-1} = \bar{\mathbf{e}}_{k-1|k-1} - \mathbf{G}\Delta\bar{\mathbf{u}}_k$$

$$\bar{\mathbf{e}}_{k-1|k-1} = \bar{\mathbf{e}}_{k-1|k-2} + \mathbf{L}(\mathbf{e}_{k-1} + \mathbf{G}\hat{\mathbf{u}}_{k-1} - \bar{\mathbf{e}}_{k-1/k-2}) \tag{28}$$

where $\mathbf{L}$ is the steady state Kalman gain which is given as a function of the covariance matrices of $\mathbf{w}_k$ and $\mathbf{m}_k$. Importing the QILC (Quadratic-criterion ILC) objective, $\Delta\bar{\mathbf{u}}_k$ is calculated to satisfy

$$\min_{\Delta\bar{\mathbf{u}}_k} \frac{1}{2}\left\{\left\|\bar{\mathbf{e}}_{k|k-1}\right\|_{\mathrm{Q}}^2 + \left\|\Delta\bar{\mathbf{u}}_k\right\|_{\mathrm{R}}^2\right\} \tag{29}$$

The unconstrained solution to (29) is

$$\Delta\bar{\mathbf{u}}_k = \mathbf{H}\bar{\mathbf{e}}_{k-1|k-1} = (\mathbf{G}^{\mathrm{T}}\mathbf{Q}\mathbf{G} + \mathbf{R})^{-1}\mathbf{G}^{\mathrm{T}}\mathbf{Q}\bar{\mathbf{e}}_{k-1|k-1} \tag{30}$$

5.3 RFC Formulation

During the k^{th} batch, we need to determine $\hat{u}_k(t)$ which together with $\bar{u}_k(t)$ steers $y_k(t)$ to $r(t)$ coping with real-time disturbances. Since $\bar{u}_k(t)$ is a predetermined signal, it is necessary to annihilate it during the design of real-time control. For this, we first define $a_k(t)$ as

$$a_k(t+1) = Aa_k(t) + B\Delta\bar{u}_k(t) \tag{31}$$

Also we define $\Delta\tilde{x}_k \triangleq \bar{x}_k - a(t)$ and rewrite (22) with respect to $\Delta\tilde{x}_k$

$$\Delta\tilde{x}_k(t+1) = A\Delta\tilde{x}_k(t) + Kn_k(t)$$

$$\bar{y}_k(t) = C\Delta\tilde{x}_k(t) + Ca_k(t) + \bar{y}_{k-1}(t) + n_k(t) \tag{32}$$

It is reasonable to replace $\bar{y}_{k-1}(t)$ with $\bar{y}_{k-1|k-1}(t)$ which is estimated during the ILC calculation after the $k-1^{th}$ run. Combining (21) and (32), we obtain

$$\begin{bmatrix} \hat{x}_k(t+1) \\ \Delta\tilde{x}_k(t+1) \end{bmatrix} = \begin{bmatrix} A & 0 \\ 0 & A \end{bmatrix}\begin{bmatrix} \hat{x}_k(t) \\ \Delta\tilde{x}_k(t) \end{bmatrix} + \begin{bmatrix} B \\ 0 \end{bmatrix}\hat{u}_k(t) + \begin{bmatrix} K\hat{v}_k(t) \\ Kn_k(t) \end{bmatrix}$$

$$y_k(t) - Ca_k(t) - \bar{y}_{k-1|k-1}(t) = \begin{bmatrix} C & C \end{bmatrix}\begin{bmatrix} \hat{x}_k(t) \\ \Delta\tilde{x}_k(t) \end{bmatrix} + \hat{v}_k(t) + n_k(t) \tag{33}$$

which can be written in a simplified form

$$z_k(t+1) = \mathbf{\Phi}z_k(t) + \mathbf{\Gamma}\hat{u}_k(t) + \zeta_k(t)$$

$$y_k(t) - Ca_k(t) - \bar{y}_{k-1|k-1}(t) = \mathbf{\Sigma}z_k(t) + \eta_k(t) \tag{34}$$

The input signal is calculated for $e_k(t)$ to satisfy the LQG criterion

$$\min_{\hat{u}_k(\cdot)} J_k = E\left\{e_k^T(N)\mathrm{Q}_N e_k(N) + \sum_{t=0}^{N-1} e_k^T(t)\mathrm{Q}e_k(t) + \hat{u}_k^T(t)R\hat{u}_k(t)\right\}$$

subject to (34) (35)

Enforcing $e_k(t) \to 0$ is equivalent to steering $y_k(t) - Ca_k(t) - \bar{y}_{k-1|k-1}(t)$ to $r(t) - Ca_k(t) - \bar{y}_{k-1|k-1}(t)$. Hence, (35) is an LQG servo problem for the output of (34) to follow $r(t) - Ca_k(t) - \bar{y}_{k-1|k-1}(t)$.

The solution is standard [15] and given as

$$\hat{u}_k(t) = -L_{fb}(t)z_k(t|t) + L_{ff}(t)b_k(t+1)$$

$$\Rightarrow u_k(t) = \Delta\bar{u}_k(t) + \hat{u}_k(t) \tag{36}$$

where $L_{fb}(t)$ and $L_{ff}(t)$ are run-invariant and can be estimated off-line: $b_k(t)$ can be calculated off-line after the $k-1^{th}$ run; $z_k(t|t)$ is given by the Kalman filter equation.

6. RESULTS AND DISCUSSION

In the previous accompanying papers[12], it has been already demonstrated experimentally as well as numerically that ILC technique is very effective in achieving precise tracking in the RTP system. To avoid exhibiting redundant results, in this paper we show the unique performance of the TBC technique and the performance of the T^4-based linear model, which will be referred to the physical model hereafter, in comparison with that of the traditional linear model which takes T as the output.

Fig. 3 is a result that was obtained under the following scenario. Through ten consecutive runs without any real-time disturbance, TBC was repeated and the wafer temperatures converged to the reference trajectory as closely as they can. At the 11th run, one of the lamps was intentionally removed. The

real-time control function in TBC tried to reject the disturbance effects and could achieve relatively good tracking performance. Though not shown here, powers of other lamps were increased to compensate the missing lamp. At the 12th run, the lamp was installed and TBC was applied again. As can be seen from the figure, the tracking performance returned to that of the 10th run as if there were no perturbation in the previous run, which implies that the effect of real-time disturbance is effectively isolated only at the 11th run by the TBC algorithm. In Fig. 4, the gap temperature (defined by the maximum temperature difference among the measurement points) of TBC based on the physical model is compared with that of the linear model-based TBC. We can see that the temperature uniformity could be remarkably improved by the physical model reducing the temperature gap by more than half on the average. This implies that the proposed physical model can more accurately represent the RTP system and is more relevant to the controller design than the linear model.

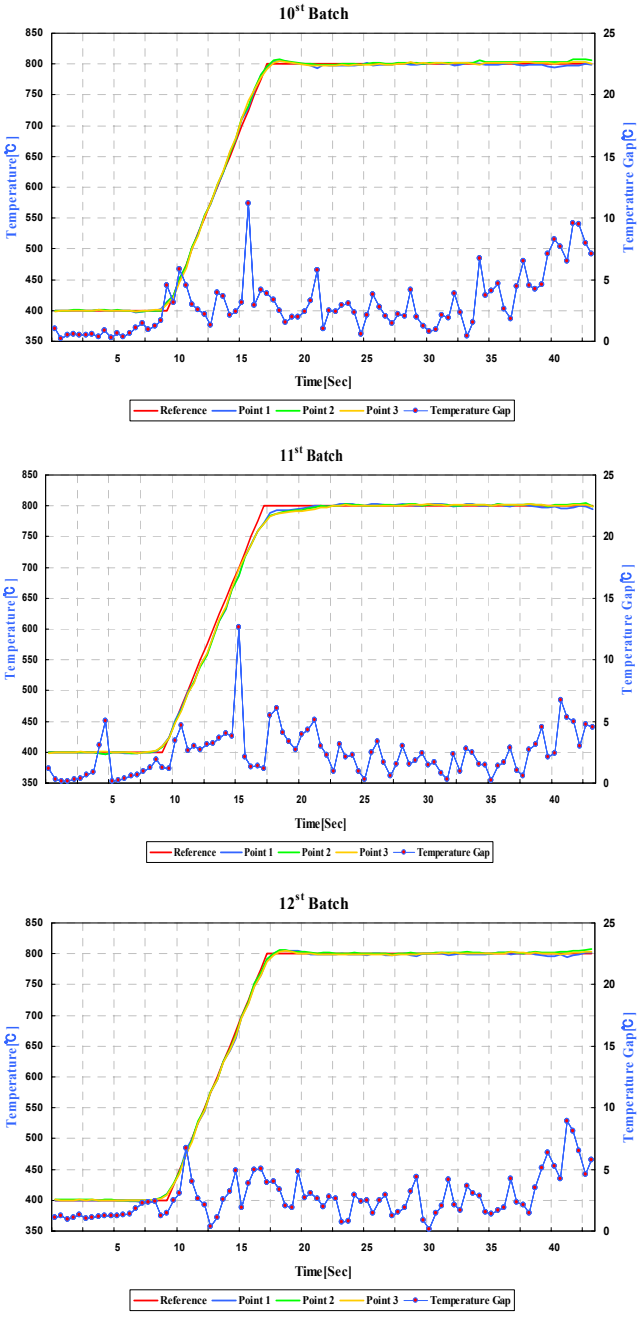

Fig. 3. Tracking performance of TBC against real-time disturbance (Real-time disturbance entered at the 11th run.).

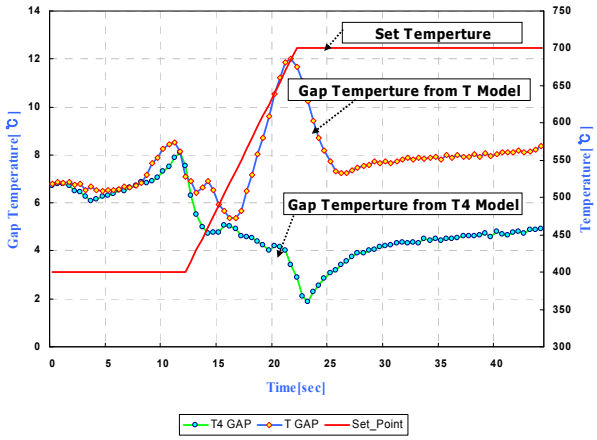

Fig. 4. Comparison of the gap temperature between linear model- based TBC and physical model-based TBC.

7. CONCLUSIONS

In this paper, a novel RTP control technique has been developed and experimentally. The novelty comes from the fact that a stat space model and LQG-based two-stage batch control (TBC) technique has been derived and implemented on the basis of a new RTP model derived from the thermal balance relationship.

Experimental application to an 8-inch RTP system showed that the TBC technique based on the physical RTP model performs better while significantly improving the temperature uniformity and attaining more accurate tracking than the previously studied, purely empirical linear model-based ILC technique. In addition, the TBC technique was found to effectively isolate the real-time disturbance effects at the batch run where the disturbance enters.

As a future research subject, further applications of the thermal balance model will be exploited such as optimal sensor location, and optimal lamp grouping and power ratio design.

ACKNOWLEDGMENTS

The authors would like to acknowledge the financial support from Korea Research Foundation and also from the Korea Science and Engineering Foundation (KOSEF).

REFERENCE

[1] T. A. Badgwell, T. Breedijk, S. G Bushman, S. W. Butler, S. Chatterjee, T. F. Edgar, A. J Toprac, and I. Trachtenberg, "Modelling and Control of Microelectronics Materials Processing", *Computers Chem. Engng,* Vol. 19 (1), 1995

[2] F. Y. Sorrell, M. J. Fordham, Ozurk, and J. J. Wortman, "Temperature Uniformity in RTP Furnaces", *IEEE Trans. Electron. Dev.*, Vol. 39, 75, 1992.

[3] R. S. Gyurcsik, T. J. Riley, and F. Y. Sorrell, "A Model

for Rapid Thermal Processing: Achieving Uniformity Through Lamp Control", *IEEE Trans. Semicond. Manuf.*, Vol. 4, 9, 1991.

[4] J. M. Dilhac, C. Ganibal, J. Bordeneuve, and N. Nolhier, "Temperature Control in a Rapid Thermal Processor", *IEEE Trans. Electron. Dev.*, Vol. 39, 201, 1992.

[5] J. D. Stuber, I. Trachtenberg, and T. F. Edgar, "Model-Based Control of Rapid Thermal Processes", *Proc. IEEE Conf. on Dec. and Contr.*, Vol. 1, 79, 1994.

[6] T. Breedijk, T. F. Edgar, and I. Trachtenberg, "A Model Predictive Controller for Multivariable Temperature Control in Rapid Thermal Processing", *Proc. Amer. Control Conf.,. San Fransisco*, 2990, 1993.

[7] P. J. Gyugyi, Y. M. Cho, G. Franklin, T. Kailath, and R. H. Roy, "Control of Wafer Temperature in Rapid Thermal Processing", *Proc. IEEE Conf. on Contr. Appl.*, Vol. 374, 1992.

[8] Y. M. Cho and P. Gyugyi, "Control of Rapid Thermal Processing: A System Theoretic Approach", *IEEE Trans. Contr. Sys. Tech*, Vol. 5, 644, 1997.

[9] C. D. Schaper, M. M. Moslehi, K. C. Sarawat, and T. Kailath, "Modeling, Identification, and Control of Rapid Thermal Processing Systems", *J. Electrochem. Soc.*, Vol. 141, 3200, 1994.

[10] A. Theodoropoulou, and E. Zafiriou, "Inverse Model-Based Real-Time Control for Temperature Uniformity of RTCVD", *IEEE Trans. Semicond. Manuf.*, Vol. 12, 87, 1999.

[11] K. S. Lee, J. Lee, I. S. Chin, J. H. Choi, and J. H. Lee, "Control of Wafer Temperature Uniformity in Rapid Thermal Processing Using an Optimal Iterative Learning Control Technique", *Ind. Eng. Chem. Res*., Vol. 40, 1661, 2001.

[12] K. S. Lee, H. J. Ahn, and D. R. Yang, "Experimental Application of a Quadratic Optimal Iterative Learning Control Method for Control of Wafer Temperature Uniformity in Rapid Thermal Processing," *IEEE Trans. Semicond. Manuf.,* Vol. 16, 1, 2003.

[13] K. S. Lee, J. H. Lee, I. S. Chin, and H. J. Lee, "A Model Predictive Control Technique Combined with Iterative Learning for Batch Processes", *AIChE J.*, Vol. 45, 2175, 1999.

[14] I. S. Chin, S. J. Qin, K. S. Lee, M. K. Cho, "A Two-Stage Iterative Learning Control Technique combined with Real-Time Feedback for Independent Disturbance Rejection", *Automatica., in print*, 2003.

[15] F. L. Lewis, V. L. Syrmos, Optimal Control. New York : Wiley, 1995.